

Whole Cell Active Inhibitors of Mycobacterial Lipoamide Dehydrogenase Afford Selectivity over the Human Enzyme through Tight Binding Interactions

John Ginn, Xiuju Jiang, Shan Sun, Mayako Michino, David J. Huggins, Zodwa Mbambo, Robert Jansen, Kyu Y. Rhee, Nancy Arango, Christopher D. Lima, Nigel Liverton, Toshihiro Imaeda, Rei Okamoto, Takanobu Kuroita, Kazuyoshi Aso, Andrew Stamford, Michael Foley, Peter T. Meinke, Carl Nathan, and Ruslana Bryk*



Cite This: *ACS Infect. Dis.* 2021, 7, 435–444



Read Online

ACCESS |



Metrics & More



Article Recommendations



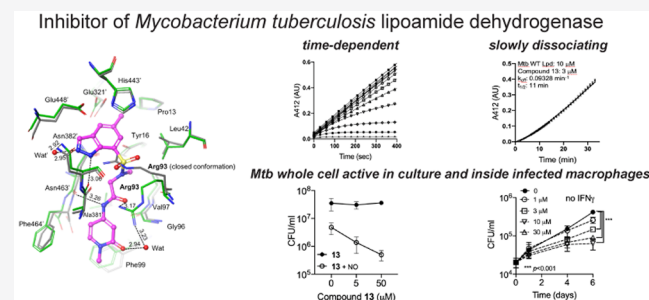
Supporting Information

ABSTRACT: Tuberculosis remains a leading cause of death from a single bacterial infection worldwide. Efforts to develop new treatment options call for expansion into an unexplored target space to expand the drug pipeline and bypass resistance to current antibiotics. Lipoamide dehydrogenase is a metabolic and antioxidant enzyme critical for mycobacterial growth and survival in mice. Sulfonamide analogs were previously identified as potent and selective inhibitors of mycobacterial lipoamide dehydrogenase *in vitro* but lacked activity against whole mycobacteria. Here we present the development of analogs with improved permeability, potency, and selectivity, which inhibit the growth of *Mycobacterium tuberculosis* in axenic culture on carbohydrates and within mouse primary macrophages. They increase intrabacterial pyruvate levels, supporting their on-target activity within mycobacteria. Distinct modalities of binding between the mycobacterial and human enzymes contribute to improved potency and hence selectivity through induced-fit tight binding interactions within the mycobacterial but not human enzyme, as indicated by kinetic analysis and crystallography.

KEYWORDS: tuberculosis, mycobacteria, lipoamide dehydrogenase, residence time, slow binding, tight binding, inhibitor

Tuberculosis (TB) infected 10 million and killed 1.5 million people in 2018.¹ It remains a worldwide health crisis due to rising drug resistance and emerging risk factors, such as diabetes. The resistance of *Mycobacterium tuberculosis* (Mtb) to all first-line anti-TB drugs is prevalent worldwide and calls for new strategies to develop effective therapeutics. The BPaL regimen recently approved by the FDA for the treatment of extensively drug-resistant (XDR) and nonresponsive multi-drug-resistant (MDR) TB features, for the first time in many decades, drugs against new Mtb targets and with novel modes of action. Nevertheless, more inhibitors against previously unexplored targets are urgently needed to sustain the TB drug pipeline and to shorten and diversify drug regimens, as resistance is already detected to components of BPaL.

Lipoamide dehydrogenase (Lpd) fulfills multiple metabolic functions and a unique antioxidant function in Mtb. It is a component of the pyruvate, α -ketoglutarate, and branched chain ketoacid dehydrogenase complexes^{2,3} involved in the breakdown of ketoacids coupled with the production of energy-rich acyl-CoA intermediates and NADH. In the reverse direction, Lpd supplies reducing equivalents from NADH through the lipoylated E2 cores of metabolic complexes to the



thioredoxin-like adaptor AhpD and the peroxiredoxin AhpC to detoxify reactive nitrogen and oxygen intermediates.^{4,5} Mtb lacking Lpd fails to grow on carbohydrates as a sole carbon source *in vitro*, cannot establish TB infection in mice, is highly susceptible to reactive nitrogen intermediates, and accumulates an ~100-fold excess of intracellular pyruvate, alanine, valine, leucine, isoleucine, and their corresponding ketoacids.³ The dependence of Mtb on Lpd for virulence and persistence provides genetic validation of Lpd as a target, but chemical validation remains to be achieved.

Bacterial enzymes with human homologues are often viewed as unattractive targets due to possible host toxicity. Although the three-dimensional structures of the mycobacterial and human enzymes align closely,⁶ mycobacterial Lpd is only 33%

Bacterial enzymes with human homologues are often viewed as unattractive targets due to possible host toxicity. Although the three-dimensional structures of the mycobacterial and human enzymes align closely,⁶ mycobacterial Lpd is only 33%

Received: November 9, 2020

Published: February 2, 2021



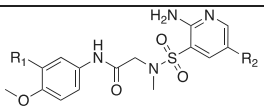
identical to the human homologue with pronounced differences in their substrate binding sites. This has allowed us to discover Lpd inhibitors with high species selectivity.^{7,8} These inhibitors were potent against the isolated enzyme but inactive against whole Mtb due to poor intrabacterial accumulation.

Here we report the development of improved sulfonamide-based Lpd inhibitors that exhibit acceptable Mtb permeability and phenocopy *lpd* genetic deletion *in vitro*. Our lead analogs are bacteriostatic to wild-type (WT) Mtb in a growing culture and bactericidal to WT Mtb under nitrosative stress in a carbohydrate-based medium. They elevate intracellular levels of pyruvate in Mtb, supporting their on-target activity against Lpd in the pyruvate dehydrogenase complex. They inhibit the growth of Mtb within primary mouse bone marrow macrophages, confirming their species selectivity and nontoxicity to these mammalian host cells. Their high efficacy, despite relatively low accumulation inside Mtb, is attributed to the tight binding interactions within the Mtb Lpd active site with a reduced dissociation rate constant and increased residence time on the Mtb enzyme. By contrast, mammalian Lpd is much less potently inhibited and exhibits rapid dissociation of the enzyme–inhibitor complex.

RESULTS AND DISCUSSION

We previously reported the identification and initial SAR of sulfonamide-based Lpd inhibitors competitive with the lipamide substrate at the Lpd's active site.⁸ Those first-generation sulfonamide Lpd inhibitors, as exemplified by compounds **1a** and **1b** (Table 1), demonstrated low solubility

Table 1. Early Aminopyridine Analogs^a

	1a	1b	2
	R ₁ = H R ₂ = Br	R ₁ = Cl R ₂ = Br	R ₁ = Cl R ₂ = Me
Lpd IC ₅₀ (μM)	0.14	0.042	0.104
aq. Sol (μg/mL pH 6.8)	1.1	0.26	4.2
Mtb Accumulation (%)	ND	ND	4.2

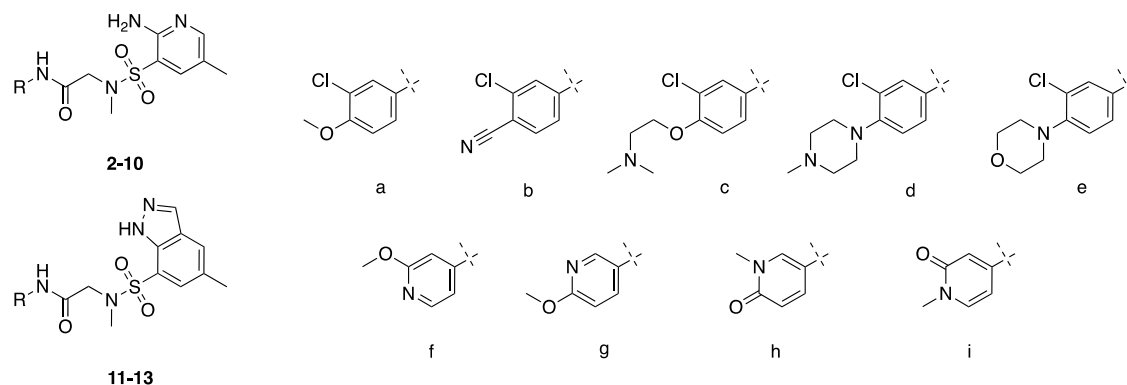
^aND, not detected. Intra-Mtb accumulation is reported as the percentage relative to the total parent compound in media during exposure.

and high metabolic instability when incubated with human liver microsomes. Poor physical properties and a propensity for metabolic clearance could have contributed to their low accumulation inside Mtb. Replacement of the pyridyl bromide by a methyl group (**2**, Table 1) improved aqueous solubility and allowed for measurable intrabacterial accumulation inside Mtb as determined by LC–MS analysis of Mtb extracts prepared from cultures exposed for 24 h to the 10 μM compound (Table 1). However, compound **2** did not demonstrate an inhibition of bacterial growth up to the maximum concentration tested, 100 μM (Table 2).

We reasoned that further modification of the physical properties may improve compound accumulation, resulting in an inhibition of bacterial growth. Compound **2** was docked into the Mtb Lpd lipoamide binding site (PDB 4MS2) using the Schrodinger GLIDE program.¹⁰ The docking pose of **2** adopted the same configuration as co-crystallized compound **1a** (Figure 1A). The extended aniline ring was oriented toward the solvent front providing a region that could be modified to

adjust physical properties without negatively impacting binding. With this in mind we initiated a SAR campaign where compounds were profiled for enzymatic potency as well as aqueous solubility and stability against liver microsomes as a general measure of a compound's metabolic stability. Mtb's waxy cell wall is notorious for its poor permeability to small molecules and poses a major challenge for antibiotic development.^{11,12} Accordingly, we also profiled all compounds for the inhibition of bacterial growth in order to identify correlations with structure or physical properties that could be used for iterative compound design efforts. Replacement of the methoxy substituent with a cyano group in **3** resulted in a significant loss in potency and reduced aqueous solubility. Extended polar substitution, as exemplified by compounds **4–6**, was well tolerated and provided improvements in both aqueous solubility and human liver microsomal stability. However, none of these compounds demonstrated the inhibition of bacterial growth. Similarly, replacement of the phenyl ring with heteroaromatic groups (**7–10**) provided compounds with desirable solubility and microsomal stability but with no inhibition of bacterial growth (Table 2). These results led us to believe that more extensive modifications would be required. As shown in Figure 1A, the sulfonamide sarcosine linker is involved in several critical hydrogen-bonding interactions, including that with the Arg93 present in Mtb but not in the human isoform. Therefore, we chose to leave that region untouched and to focus on the conserved aminopyridine core. To gain insight into the binding pocket, we characterized the binding site features using the Schrodinger SiteMap Program.⁹ The model revealed a hydrophobic area near the amino-pyridine ring suggesting that the binding pocket could be better filled (Figure 1B). In addition, only one of the amino-pyridine NH groups appeared to be important for hydrogen bonding with the enzyme (residue Ala381 in Figure 1) as well as forming an internal hydrogen bond with the sulfonamide oxygen. To this end, indazole **11** was designed by the cyclization of the amino group back onto the aromatic ring while retaining the key NH hydrogen bond donor. The profiling of **11** demonstrated an improvement in enzyme inhibition as well as whole cell activity with an MIC₉₀ of 25 μM when tested against WT Mtb grown in a carbohydrate-based medium. *In vitro* ADME-tox profiling of **11** showed that while the aqueous solubility was maintained, the compound suffered from rapid microsomal clearance. Following the SAR generated for the aminopyridines, compounds **12** and **13** were synthesized. Compound **12** demonstrated an improvement in MIC compared to that of **11** but did not maintain the improved microsomal stability associated with the morpholine substitution (compound **6**). However, *N*-methyl pyridone-substituted **13** maintained the improved properties and further increased the MIC potency to 3.1 μM in a carbohydrate-based medium.

The improved antibacterial activity of **11–13** prompted us to investigate the intrabacterial accumulation of these compounds and to measure the elevation in intracellular pyruvate. The latter serves as a biomarker of intrabacterial Lpd inhibition in accordance with the phenotype of *lpd* deletion in Mtb³ and Lpd's function in Mtb's pyruvate dehydrogenase.² Table 3 shows the fold increase in intrabacterial pyruvate levels observed after 24 h of exposure of Mtb to the 10 μM compound as well as the percentage of the parent compound associated with Mtb and remaining in the medium. The relative increase in intracellular pyruvate levels for **11–13** is

Table 2. SAR Analysis, Antibacterial Activity, and ADME Profiling of Sulfonamide Analogs^a

no.	R	Lpd IC ₅₀ (μM)	Mtb MIC ₉₀ (μM)	Sol (μg/mL, pH 6.8)	hLM (μL/min/mg)	log D
2	a	0.104	>100	4.6	115	1.85
3	b	1.70	>100	0.15	113	1.94
4	c	0.11	>100	>110	2	1.69
5	d	0.128	>100	>120	15	2.12
6	e	0.056	>100	20	18	2.12
7	f	0.196	>100	>100	-14	1.37
8	g	0.331	>100	>97	6	1.32
9	h	2.75	>100	>95	-18	0.4
10	i	0.165	>100	>97	13	0.45
11	a	0.035	25	18	>768	2.26
12	e	0.029	12	23	195	2.55
13	i	0.045	3.1	>110	-11	0.83

^aIC₅₀ values were determined by the DTNB assay with 50 nM Lpd.

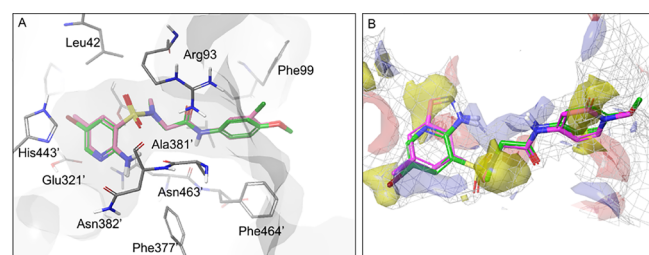


Figure 1. (A) Docking pose of compound **2** (pink) superimposed with Br analog **1a** (green) in the Mtb Lpd co-crystal (PDB 4MS2). The gray surface indicates the protein surface. (B) Overlaid docking pose of **13** (magenta) and crystal structure of **1a** (green) with SiteMap[®] predictions in the Lpd lipoamide site. Yellow indicates the hydrophobic region. Purple and red indicate hydrogen bond donor and acceptor regions, respectively.

Table 3. Intrabacterial Pyruvate Levels and Compound Accumulation in Mtb^a

compound	11	12	13
pyruvate increase (fold)	10.6 ± 0.16	25.6 ± 0.03	37.3 ± 0.05
intra-Mtb accumulation (%)	21	35	6
compound remaining (%)	41	39	85

^aFold pyruvate is relative to levels observed in untreated Mtb. Intra-Mtb accumulation and the compound remaining is the percentage relative to the total parent compound in media at the initiation of the experiment.

correlated with increased efficacy for the inhibition of bacterial growth. Compound **12**, although accumulated better in Mtb, was less efficacious than **13** in terms of intrabacterial target engagement, suggesting that other factors, such as association within the cell wall/membrane compartment or its lower

metabolic stability may have further affected its intra-Mtb bioavailability. Compound **13** emerged as the most promising lead with the lowest MIC and highest pyruvate fold increase, suggesting significant gains in target engagement even at relatively low intra-Mtb accumulation levels. This prompted us to further profile the inhibition of Lpd by compound **13**.

Compound **13** exhibited the time-dependent inhibition of purified recombinant Mtb Lpd following reaction initiation by the addition of enzyme (Figure 2A). Fitting the progress curve data to the first-order rate kinetics produced values of k_{obs} that increased with an increasing molar excess of inhibitor to Lpd (Figure 2B). The relationship was not strictly linear, suggesting an induced fit model for **13** association with Lpd. Upon 30 min of preincubation, IC₅₀ values tracked linearly with variable enzyme concentration, nearing the values for the concentrations of Lpd and suggesting a slow-onset, tight binding interaction (Figure 2C). Close tracking of IC₅₀ values with the Lpd concentration for compound **13** suggested that the determination of true K_i values through the traditional Michaelis–Menten kinetics was not possible as the tight association of the inhibitor in the Lpd–inhibitor complex limited the free concentration of compound **13** in the assay. Thus, we proceeded to calculate K_i^{app} using the steady-state rate at fixed concentrations of Lpd and the lipoamide substrate (75 μM). This inhibition data, expressed as the fractional velocity at a given inhibitor concentration, was fitted to the Morrison equation for tight binding inhibitors to calculate $K_i^{app} = 9 ± 6.9$ nM. To determine the dissociation rate of compound **13** from the Lpd–**13** complex, we preincubated Lpd with **13** and subsequently diluted the complex 500-fold into the assay mixture to follow the recovery of Lpd activity. We observed the rapid recovery of activity at subequimolar concentrations of inhibitor during preincubation and fractional recovery with a

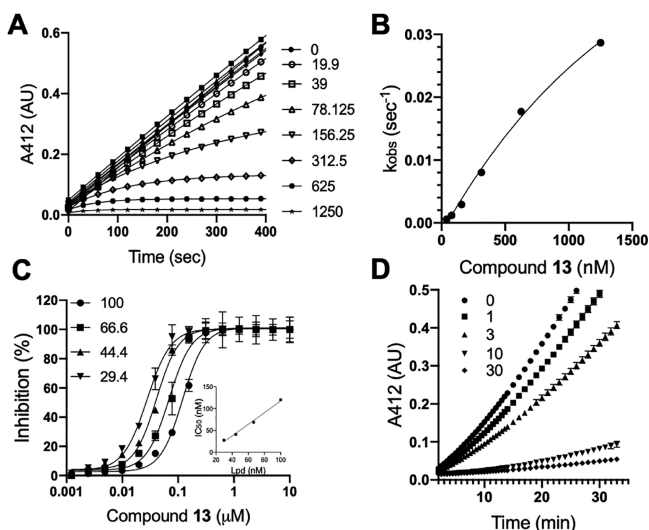


Figure 2. Compound 13 is a potent, time-dependent, slowly dissociating inhibitor of Mtb Lpd. (A) Compound 13 produces a time-dependent inhibition of Lpd activity. Pure recombinant Mtb Lpd (66 nM) was tested against variable concentrations of compound 13, and TNB product formation was followed over time at 412 nm. Each symbol corresponds to an indicated compound 13 concentration in nM. Symbols represent experimental data recorded every 30 s, and solid lines are best fits to the first-order association function. (B) First-order rate constant of inactivation (k_{obs}) increases with the compound 13 concentration. Values of k_{obs} were determined from the first-order association fit represented by a solid line in A. (C) IC_{50} values for compound 13 inhibition of Mtb Lpd depend on Lpd concentration. Lpd was tested at the indicated concentrations represented by different symbols (numbers for each symbol correspond to [Lpd] in nM) for inhibition by increasing concentrations of compound 13; the inset shows the plot of [Lpd] vs calculated IC_{50} . (D) Recovery of Lpd activity upon dilution of the Lpd-13 complex. Lpd (10 μM) was preincubated with the indicated μM concentrations of 13 for 30 min at RT, diluted 500-fold into the reaction mixture with 75 μM lipoamide and monitored for TNB formation over time.

long lag period at a molar excess of 13 (Figure 2D). Fitting the recovery experimental data for compound 13 to the integrated rate equation to determine the dissociation rate constant¹³ produced a k_{off} value of 0.084 min^{-1} , which corresponded to a 12 min half-life ($t_{1/2}$) for the Lpd-13 complex (Figure S1). At equimolar and higher concentrations of compound 13, the recovery slowed, with a >10-fold reduction in k_{off} values corresponding to hours-long $t_{1/2}$ (Figure S1). This sustained inhibition at higher concentrations likely reflected the continuous rebinding of the dissociated (and/or excess) inhibitor. Nevertheless, enzymatic data suggested an extended residence time of 13 on Mtb's Lpd under conditions at which 13 is present in molar excess with respect to Lpd. Thus, achieving intra-Mtb levels of 13 in excess of Lpd intracellular concentration should result in sustained target engagement and drive the inhibition of Lpd activity *in vivo*.

In contrast, when compound 13 was tested against the recombinant human Lpd in a similar manner, no time-dependent inhibition was observed (Figure 3A), the IC_{50} values did not change significantly with variable enzyme concentration (Figure 3B), and inhibition was rapidly reversible upon dilution, even at a high molar excess of inhibitor (Figure 3C). Taken together, these results demonstrate that 13 is a significantly less potent ($K_i^{\text{app}} = 1.13 \pm 0.18 \mu\text{M}$) rapid equilibrium inhibitor of human Lpd.

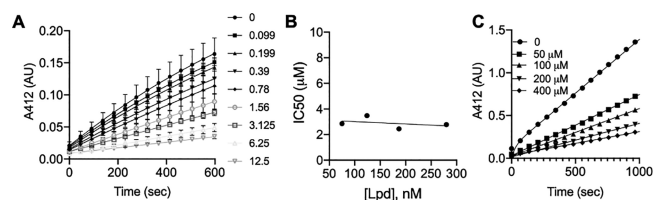


Figure 3. Compound 13 is a readily reversible inhibitor of human Lpd. (A) The activity of human Lpd (280 nM) was monitored over time in the presence of the indicated micromolar concentrations of 13. (B) IC_{50} values were calculated at variable Lpd (75, 124, 187, and 280 nM) and plotted against [Lpd]. (C) Human Lpd (10 μM) was preincubated with the indicated micromolar concentrations of 13 for 30 min at RT, diluted 125-fold into the reaction mixture with 75 μM lipoamide, and monitored for TNB formation over time.

Increased inhibition rates with excess 13 suggested the possibility of an induced fit model that may have contributed to the high affinity and slow dissociation of 13 when all active sites are occupied by an inhibitor. We examined the crystal structures of Mtb Lpd with and without 13 for conformational changes within the lipoamide binding pocket or in its vicinity upon the binding of 13 and identified the only significant structural change in the Arg93 conformation. The original crystal structure of Mtb Lpd⁶ identified Arg93 as being able to adopt two different conformations within the lipoamide channel by positioning its side chain to stack above His386' for open access to the channel (open conformation) or to protrude into the channel and block access (closed conformation). The Lpd co-crystal with 13 adopted the open conformation⁶ to accommodate bound 13 (Figure 4).

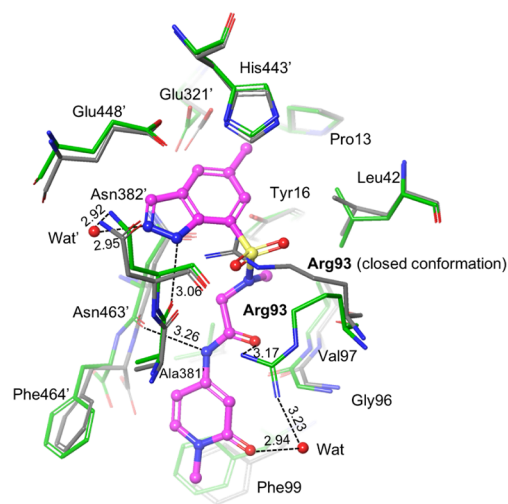


Figure 4. Co-crystal structure of Lpd (green) with 13 (magenta) superimposed with the Lpd apo structure⁶ (PDB 2A8X, gray). Dotted lines indicate the distance in angstroms.

Compound 13 occupies each of the two lipoamide binding channels, which are formed between the protomers. The indazole ring sits deep within each channel and is in close proximity to the disulfide-based redox center adjacent to His443' and Glu448'. A direct hydrogen bond is observed between the indazole NH and the Ala381' backbone carbonyl. In addition, a water-mediated hydrogen bond forms between the indazole ring and the side-chain amide of Asn382'. The 5-position methyl group of 13 sits in a hydrophobic pocket pointing toward Pro13. Similar to the previous aminopyridine

analog **1a**,⁸ the Arg93 side chain swings out to adopt an open conformation (Figure S2). The amide group of **13** interacts with both the Arg93 guanidinium and the backbone carbonyl oxygen of Asn463', which are believed to be important for imparting both potency and selectivity to human Lpd. At the solvent-exposed end of the channel, the pyridone carbonyl of **13** forms a water-mediated hydrogen bond with the Arg93 side chain, which orients the pyridone ring for π - π stacking with Phe99.

The crystal structure of Mtb Lpd suggested a critical role for Arg93 in maintaining access to the lipoamide binding site as it was able to adopt two different conformations.⁶ The co-crystal of Lpd with **13** identified Arg93 among contact residues and demonstrated that Arg93 adopts an open conformation upon **13** binding. Human Lpd has a Leu residue at that position, and the lack of coordination through Arg93 may have contributed to the lower affinity of **13** for the human homologue. We tested an Mtb Lpd mutant enzyme with single amino acid substitution R93A to determine if Arg93 contact contributes to the binding affinity and affects the dissociation rate of **13**. No time-dependent inhibition of Mtb Lpd R93A activity in the presence of **13** was observed, progress curves with increasing **13** concentrations were linear from the onset (Figure 5A), and

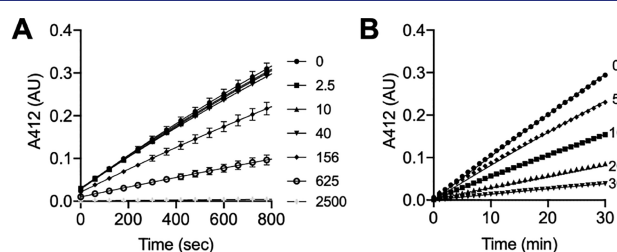


Figure 5. Compound **13** is a rapid equilibrium inhibitor of the Mtb Lpd R93A mutant. (A) Progress curves for Lpd R93A (200 nM) at the indicated nanomolar concentrations of **13**. Reaction was initiated by enzyme addition. (B) Lpd R93A (10 μ M) was preincubated with the indicated concentrations of **13** (in μ M), diluted 125-fold into the reaction mixture with 75 μ M lipoamide, and monitored for TNB formation over time.

K_i^{app} was calculated to be 218 nM. Lpd R93A preincubation with **13** and dilution into the assay mixture to recover the activity resulted in linear progress curves without any lag, suggesting the rapid dissociation of **13** from Mtb Lpd R93A (Figure 5B).

Enzyme kinetics suggested that compound **13** is a potent inhibitor of Mtb Lpd and that Arg93 is important for this tight association. To learn more about what was driving this tight association, we performed ITC and SPR profiling for both the WT and the R93A Mtb Lpd as well as the human Lpd interaction with compound **13** (Figures S3–S6). We observed that the affinity of compound **13** for WT Mtb Lpd depended on the presence of NADH and was in good agreement with the K_i^{app} values calculated through enzyme inhibition assays. Thus, the K_d for the WT Lpd decreased more than 2-fold in the presence of NADH, suggesting a possible conformational adjustment within the lipoamide site upon the binding of NADH that resulted in a tighter association with compound **13** (Table 4). The NADH-dependent change in the shape of the lipoamide channel upon its binding may explain why we were unable to identify any additional differences except for the Arg93 conformation in the crystal structures upon **13** binding, as both structures were crystallized in the presence of NADH. The R93A mutant bound compound **13** in an NADH-independent manner with $K_d = 227 \pm 6.6$ nM, which was in agreement with the K_i^{app} calculated from enzyme inhibition data. Thus, it appeared that R93 contact contributes to the binding affinity and may adjust its conformation upon **13** and/or NADH binding, which is consistent with its conformational flexibility in the Mtb Lpd crystal structure.⁶ The human Lpd bound compound **13** with a much lower affinity, and in some repeats we were not able to fit the data properly. The binding of compound **13** to the WT Mtb Lpd was mostly enthalpy-driven, suggesting hydrogen-bonding involvement (Figure S5).

Similarly, the kinetic analysis of compound **13** binding to WT Mtb Lpd by SPR produced K_d values close to the ones observed by ITC, but we did not observe a significant dependence of the binding affinity on the NADH presence. This could reflect a difference in the Lpd native conformation as a dimer, which was preserved in ITC but could have been disrupted in the SPR by the covalent immobilization of Lpd. Best fitting of the kinetic binding data was achieved with the two-state model, which had fast on/off and slow on/off components in the absence of NADH. In the presence of NADH, the fast on/off component converted to the fast on/slow off site with slow dissociation corresponding to a 40-fold increase in the half-life of the Lpd–**13** complex (Table 4, Figure S6). The SPR values for k_{off} agreed well with the numbers calculated from rapid dilution experiments. Human Lpd protein produced K_d in the micromolar range and faster

Table 4. Characterization of **13** Binding to Lpd by ITC and SPR^a

	ITC		SPR		
	K_d , nM	K_d , nM	k_{on} , $\text{M}^{-1} \text{s}^{-1}$	k_{off} , s^{-1}	$t_{1/2}$, min
Mtb WT	63.9 ± 2.75	52.3	35 500 (1) 0.0177 (2)	0.0315 (1) 0.0011 (2)	0.5 (1) 15.15 (2)
Mtb WT/NADH	28.3 ± 1.74	44.5	18 500 (1) 0.00000222 (2)	0.00083 (1) 0.00158 (2)	20.15 (1) 10.5 (2)
Mtb R93A	231.4 ± 8.81	ND	ND	ND	ND
Mtb R93A/NADH	228.6 ± 2.44	ND	ND	ND	ND
human WT	592	7600	1170	0.00887	1.9
human WT/NADH	ND	ND	110	0.00628	2.7

^aND, not determined. K_d values were calculated by using the stoichiometric equilibria model assuming $A + B \leftrightarrow AB$ (ITC) and the two-state model assuming complex AB undergoes a conformational change: $A + B \leftrightarrow AB \leftrightarrow AB^*$ (SPR; $k_{\text{on}}(1)$ is the association rate constant for the formation of AB; $k_{\text{off}}(1)$ is the dissociation rate constant for complex AB; $k_{\text{on}}(2)$ is the association rate constant for the conversion of AB to AB*; and $k_{\text{off}}(2)$ is the dissociation rate constant for the conversion of AB to AB*). Results are representative of two independent repeats.

dissociation rates by SPR with a half-life of 2 min, confirming its lower affinity and 10-fold higher dissociation rates for compound **13**. These results are consistent with our enzymatic data analysis and support the interpretation that Mtb's Lpd binds **13** tightly through an induced fit model in the presence of NADH. This scenario will likely play out inside Mtb *in vivo* as the mycobacterium maintains high nanomolar to low micromolar NADH levels throughout different stages of its growth cycle.^{14–16} Human Lpd will be spared from inhibition due to its lower affinity for **13**, aided by the rapid dissociation of the human Lpd–**13** complex.

We speculated that the tight binding and relatively slow dissociation of **13** from Mtb Lpd drove the whole cell activity of **13** against Mtb even at relatively low intrabacterial accumulation levels. Accordingly, we decided to examine whether treatment with **13** could reproduce any of the other phenotypes associated with the *lpd* genetic deletion in Mtb. In accordance with the high susceptibility of Δ *lpd* Mtb to nitrosative stress,³ where 99% of Δ *lpd* Mtb is killed upon exposure to 3 mM NaNO₂ at pH 5.5 (NaNO₂ generates a flux of NO at acidic pH), **13** proved to be bactericidal in a concentration-dependent manner to WT Mtb at pH 5.5 in the presence of 3 mM NaNO₂ but had no effect at the same concentrations when Mtb was exposed to pH 5.5 alone (Figure 6A). Mtb Δ *lpd* does not replicate in naïve mouse bone

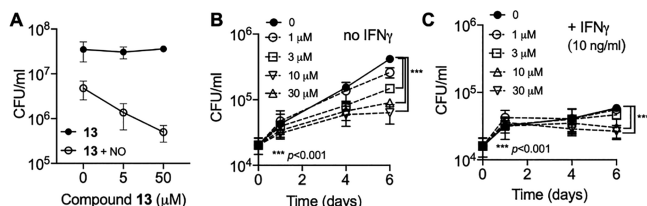


Figure 6. Compound **13** selectively kills Mtb under nitrosative stress and inhibits the growth of Mtb inside mouse BMDM. (A) WT Mtb was exposed to pH 5.5 or pH 5.5 plus 3 mM NaNO₂ in the presence of **13** for 4 days and plated on agar to enumerate colony-forming units (CFU) of surviving bacteria. (B) Mouse BMDMs were infected with WT Mtb (multiplicity of infection (MOI) = 0.1) and exposed to the indicated μ M concentrations of **13**. At the indicated time points, BMDM were lysed and CFU were determined. (C) The same as in B, but BMDM were activated with 10 ng/mL IFN γ for 24 h prior to infection. Results are the means \pm SD of triplicate wells in a single experiment representative of two independent experiments. *P* values were calculated with an unpaired *t* test.

marrow-derived macrophages (BMDM) and dies by 1 log₁₀ in BMDM activated by interferon- γ (IFN γ).³ Compound **13** inhibited the growth of WT Mtb in naïve BMDM in a concentration-dependent manner, recapitulating the Mtb Δ *lpd* phenotype. By day 6 after infection, treatment with **13** inhibited the growth of Mtb by 1 log₁₀ in naïve BMDM and by 0.5 log₁₀ in IFN γ -activated BMDM at the highest concentration tested, 30 μ M.

No toxicity to mouse BMDM was observed at any concentration of **13** tested as assessed by the MTS assay, suggesting that the prolonged residence time of **13** on Mtb's Lpd selectively contributed to increased vulnerability of Mtb to Lpd inhibition inside mammalian host cells. Similarly, the profiling of **13** in HEPG2 cells showed no signs of cytotoxicity up to 100 μ M, consistent with the efficacy in the BMDM experiment being driven through on-target activity in Mtb.

Slowly reversible, tight binding enzyme inhibitors offer the benefits of both enhanced potency and prolonged on-target residence time, extending their pharmacologic effect *in vivo*.¹⁷ Our work reports on a first in class, slowly dissociating, high-affinity inhibitor of Mtb Lpd, which is whole cell active, recapitulates phenotypes of *lpd* genetic deletion in Mtb, and affords high selectivity over the human homologue due to its tight binding induced-fit interaction with Arg93 within the Mtb lipoamide substrate binding site but not the human enzyme. Tight binding of compound **13** to Mtb's Lpd may be aided by NADH binding to Lpd and/or may reflect conformational adjustments within the lipoamide channel or its desolvation upon **13** binding to achieve tighter contacts.

In vitro, compound **13** demonstrated comparable potency against Lpd in singularity or as a component of a larger PDH complex (in the presence of recombinant E2 = D1aT and E1 = AceE proteins), suggesting that the Lpd conformation, or at least the architecture of the lipoamide channel, is similar under both conditions. However, *in vitro* data cannot fully predict how efficacious such an inhibitor will be when it encounters a target in its natural milieu, where physiological protein expression, turnover, and posttranslational modification levels (E2 cores of PDH and BCKDH present covalently attached lipoamide to Lpd) as well as other substrate levels (e.g., NAD⁺/NADH) may affect the affinity and on-target residence time to define the *in vivo* target vulnerability. Our studies on whole cell Mtb in axenic culture, under nitrosative stress or inside mouse BMDM, demonstrate that, despite its low accumulation inside Mtb, compound **13** effectively targets intracellular Lpd functions in PDH and BCKDH. This is demonstrated by the accumulation of pyruvate and branched-chain amino acids (isoleucine, leucine, and valine) inside Mtb exposed to compound **13**, the selective killing of Mtb under nitrosative stress, and the inhibition of Mtb growth inside mouse BMDM. High levels of pyruvate accumulation inside Mtb despite limited **13** accumulation suggest that tight binding and slow dissociation features of **13** are likely to manifest under physiological intracellular levels of NAD⁺/NADH inside Mtb and that intracellular or local concentrations of compound **13** likely reach levels equimolar with or higher than intracellular Lpd levels to sustain on-target activity. Alternatively, Lpd assembly into the large intracellular complexes may aid the maintenance of highly concentrated local pools of dissociated inhibitor in close proximity to other Lpd active sites, promoting rebinding¹⁷ and sustained on-target residence.

One can argue that the sustained inhibition of enzymatic activity may lead to the generation of resistance mechanisms to overcome the inhibition through mutations within the Lpd protein or upregulation of bypass metabolic routes. We are in the process of determining the frequency of resistance for the indazole analogs and plan to systematically identify resistant mutants if such arise upon treatment of Mtb in culture or in mice with compound **13** or its improved analogs.

Our future analogs will further explore the binding site to identify water molecules which could be displaced to facilitate higher-potency interactions and improve on-target residence time. Our data demonstrates that Arg93 is critical to maintaining tight interactions within the binding site; therefore, we will preserve those contacts but explore the distal pocket to pick up new contacts. We will also target improved *in vivo* efficacy by identifying compounds that accumulate better inside Mtb to maintain full target occupancy as well as having improved PK. Testing such an inhibitor in an animal model of

TB may offer the best way to confirm the vulnerability of Mtb to Lpd chemical inhibition in a mammalian host. Compound 13 was not tested for efficacy in the mouse model of TB because it is highly susceptible to mouse microsomal metabolism and most likely would not be able to achieve suitable target coverage over the course of the experiment. However, our present results support the rationale of efforts to improve bacterial accumulation and metabolic stability while preserving tight binding for Mtb Lpd to develop analogs suitable for testing *in vivo*.

Tight binding interactions have been explored in the development of antibiotics against other bacterial targets, such as dihydrofolate reductase,¹⁸ zinc-dependent deacetylase of lipid A biosynthesis,¹⁹ bacterial and insect trehalases,²⁰ and proteases. The residence time of macrolide antibiotics on ribosomes was reported to define their antibacterial whole cell activity, with slowly dissociating macrolides being cidal and rapidly dissociating macrolides resulting in bacteriostasis.²¹ The residence time of macrolide antibiotics on the bacterial ribosome²² was recently correlated with their post-antibiotic effect to build a model that demonstrates the dependence of the post-antibiotic effect on the target residence time. A similar approach was undertaken to predict the *in vivo* efficacy of UDP-3-O-acyl-N-acetylglucosamine deacetylase inhibitors.²³ These examples underscore the utility of tight binding and slowly dissociating inhibitors in antibiotic development for target vulnerability validation and the prediction of *in vivo* efficacy.

In summary, our results demonstrate that Mtb's Lpd is vulnerable to chemical inhibition in axenic Mtb cultures and inside Mtb-infected mouse primary macrophages under the conditions where intrabacterial levels of reactants and protein turnover are maintained. Improved analogs with longer residence times could reveal further gains in *in vivo* efficacy, leading to studies on Mtb's Lpd vulnerability to small-molecule inhibition in acute and chronic models of TB infection.

METHODS

General. All chemicals were from Sigma. Recombinant protein production and purification (Mtb Lpd WT and Mtb Lpd R93A) was performed as reported previously.⁸ Purified recombinant human Lpd was a generous gift from Prof. M. Patel, University at Buffalo, SUNY. Lpd activity was measured by the DTNB assay according to previously published procedures.⁸ For the preincubation of Lpd with the inhibitor, Lpd was dispensed into the wells, and compounds were added at specified concentrations, mixed, and preincubated at RT for 30 min without any other components. Reaction was started by adding the assay mixture containing the substrates (lipoamide, NADH) and DTNB, and TNB production was recorded over time at RT in the SpectraMax plate reader at 412 nm. For time-dependent measurements, compounds were added to wells containing the assay mixture, the reaction was started by the addition of Lpd protein, and TNB production was followed over time in the SpectraMax plate reader at 412 nm. Final concentrations of components in the reaction mixture were as follows: 150 μ M NADH, 150 μ M DTNB, 40 μ M NAD⁺, 75 μ M lipoamide in 25 mM potassium phosphate, and 1 mM EDTA pH 7.0. The Lpd protein was tested at variable concentrations specified in the graphs. The protein concentration was determined by the Bradford assay kit (Sigma), the Lpd concentration is provided for the monomeric enzyme; the active species is a dimer and binds 2 molecules of compound

per dimer. Progress curves were fitted to first-order association in GraphPad Prism to calculate k_{obs} . K_i^{app} for tight binding inhibitors were calculated in GraphPad Prism by fitting the fractional velocity data to the Morrison K_i^{app} equation $Y = Vo(1 - (((Et + X + (K_i(1 + (S/K_m)))) - (((Et + X + (K_i(1 + (S/K_m))))^2 - 4EtX)^{0.5})/(2Et)))$ where $Et = 66$ nM, $S = 75$ μ M, and $K_m = 50$ μ M. The K_i^{app} values for R93A and human Lpd proteins were calculated by using the equation $K_i = IC_{50}/(S/K_m + 1)$ for a competitive inhibitor.

MIC Assay. MIC values were determined on the WT *Mycobacterium tuberculosis* H37Rv strain in 96-well plates in 200 μ L of Middlebrook 7H9 medium at pH 6.6 with 0.2% glycerol, 0.02% tyloxapol, and 10% ADN (5% fatty acid-free BSA (Roche), 2% dextrose, and 0.85% NaCl). The starting bacterial inoculum was 0.01 (OD₅₈₀). Inhibitors were tested at 2-fold serial dilutions from 100 to 0.1 μ M. Growth was evaluated by the change in OD₅₈₀ after 10 days of incubation at 37 °C in 5% CO₂, 95% humidified air. Blank wells (0% growth) contained 200 μ L of medium; control wells without inhibitor were defined as having 100% growth. Growth in experimental wells with inhibitors was calculated as the percentage relative to no inhibitor controls. MICs were defined as compound concentrations that inhibited bacterial growth of >90%.

Determination of Inhibitor Mtb Intracellular Accumulation by Metabolic Profiling. WT H37Rv Mtb was grown in 7H9 Middlebrook medium supplemented with 0.2% glycerol, 0.2% dextrose, 0.5% BSA, 0.085% NaCl, and 0.02% tyloxapol to an OD₅₈₀ of 1.0. One milliliter of culture at OD₅₈₀ = 1.0 was filtered through a nitrocellulose membrane (0.22 μ M; Millipore GSWP 02500). Mtb-laden membranes were placed atop "swimming pools" constructed from inverted 15 mL falcon tube caps filled with media. Samples were incubated at 37 °C in 5% CO₂ for 7 days to accumulate biomass and checked daily to ensure that membranes were in constant contact with the growth medium. Membranes were then transferred to fresh media-based pools with or without 10 μ M compound for 24 h. Filters were flipped into a 1 mL ice-cold 40:40:20 solution of methanol/acetonitrile/water. Mtb was scraped off the filters and lysed via bead beating three times. Small-molecule extracts were mixed 1:1 with an acetonitrile/0.2% formic acid solvent for MS analysis. To determine compound intracellular accumulation, a standard curve was generated by spiking a mycobacterial small-molecule extract with known concentrations of compound to correct for the ion suppressive effects of lysate. To assess the metabolite abundance, protein was measured using a Pierce BCA kit, and ion counts of specified metabolites were normalized to protein concentration.

BMDM. BMDM were differentiated as reported²⁴ for 6 to 7 days in complete DMEM (4.5 g/L glucose, 10% FBS, 1% HEPES, 1% sodium pyruvate, and 1% L-glutamine) supplemented with 20% L929 cell-conditioned medium (LCM). Cells were collected in 0.5 mM EDTA in PBS, washed with 10% LCM in complete DMEM, counted with a hemocytometer, and plated in 48-well plates [(2.0–2.5) $\times 10^5$ cells/well] in 0.5 mL 10% LCM in complete DMEM. No antibiotics were used at any stage in any experiments. All cultures were incubated at 37 °C in a mixture of 5% CO₂ and 95% humidified air. Isolation of bone marrow macrophages from mice was performed in accordance with NIH guidelines for the housing and care of laboratory animals and WCM institutional regulations after protocol review and approval by the

Institutional Animal Care and Use Committee (IACUC protocol 2013-0001).

Infection of BMDM with Mtb. BMDM were plated in 48-well plates $[(2.0\text{--}2.5) \times 10^5$ cells/well] in 0.5 mL of 10% LCM in complete DMEM. Where indicated, mouse IFN γ (final 10 ng/mL, Roche) was added and cells were left to adhere overnight. A single-cell suspension of Mtb H37Rv in PBS with 0.02% tyloxapol was added in 50 μ L to achieve an MOI of 0.1. Four hours later, the medium was removed, the monolayers were washed twice with warm PBS, and 0.5 mL of fresh 10% LCM in complete DMEM was replaced. BMDM were observed daily, and photomicrographs were recorded. Only wells with intact BMDM monolayers were used for the determination of CFU. Test agents were added 24 h after Mtb infection by replacing the medium in wells with BMDM with 10% LCM in complete DMEM containing the indicated final concentrations of inhibitors. Data are presented according to the time after treatment as opposed to the time after infection. At each time point, the medium was removed, and monolayers washed with warm PBS and BMDM were lysed with 100 μ L of 0.5% Triton X100 in PBS. PBS (400 μ L) was immediately added to wells to dilute the Triton X100 to 0.1% to minimize any impact on Mtb viability. Samples were serially diluted, and 10 μ L was plated on 7H11 agar plates incubated at 37 $^{\circ}$ C for CFU enumeration 3 weeks later.

Crystallization and Structure Determination. Mtb Lpd expression and purification for crystallographic analysis were performed as reported.^{6,8} Lpd (200 μ M), inhibitor **13** (300 μ M), and 600 μ M NADH were mixed and incubated on ice for 10 min prior to crystallization at 18 $^{\circ}$ C by hanging drop vapor diffusion against a well solution containing 100 mM Tris at pH 8.5, 50 mM NaCl, 15% PEG 10000 (w/v), and 14% glycerol. Crystals were cryo-protected by the addition of 25% glycerol and flash cooled in liquid nitrogen. A single crystal was diffracted and data were collected at NE-CAT beamline 24-IDC at 0.9791 \AA to obtain a data set at 2.2 \AA resolution. The structure of Lpd bound to **13** was determined by molecular replacement using programs contained within CCP4 and our previously determined structure of Lpd.⁶ The crystal lattice included four dimers in the asymmetric unit and a model comprising Lpd amino acids 1–464 and an additional N-terminal Ser residue that remained from the cleavage tag (Gly-Ser). This model was refined using Phenix²⁵ after manual rebuilding in Coot.²⁶ Water molecules (1560) and **13** were added to the model and refined to an R/Rfree of 0.189/0.221 at 2.2 \AA . Densities within the NADH binding site could not be modeled reliably with NADH, so densities were fit with solvent atoms. The model has excellent geometry, with 96.5 and 3.5% of residues in favored and allowed regions of Ramachandran space with MolProbity scores for all atom contacts and protein geometry in the 100th percentile for both regions.²⁷ Atomic coordinates and structure factors have been deposited in the Protein Data Bank with accession code 7KMY.

ITC Measurements. All measurements were performed on a MicroCal Auto-ITC200 instrument. Lpd was used at 10 or 20 μ M, and compound **13**, at 250 μ M. Measurements were performed in a mixture of 25 mM potassium phosphate buffer at pH 7.0 and 2.5% DMSO \mp 100 μ M NADH or in a mixture of 20 mM triethanolamine buffer at pH 7.8 and 2.5% DMSO \mp 100 μ M NADH. Data analysis was performed with Affinimeter software using the stoichiometric equilibria model assuming free species $\leftrightarrow A_1B_1$. K_d was calculated as a reciprocal of K_a . The free energy was calculated with $\Delta G = RT \ln K_d$, where $R =$

1.9858775 cal $M^{-1} K^{-1}$ and $T = 298.15$ K. $T\Delta S$ was calculated with

$$\Delta G = \Delta H - T\Delta S$$

SPR. All measurements were performed on the eight-needle high-sensitivity SPR Biacore 8K system (Cytiva). A CM5 sensor chip was used for all experiments. Mtb and human WT proteins were immobilized on the matrix via amine coupling at pH 5.0 to achieve comparable RUs ($11\,342 \pm 58.96$ for Mtb and $12\,735 \pm 125.49$ for human Lpd). Parallel kinetics was run in a mixture of 25 mM potassium phosphate at pH 7.0, 0.05% surfactant P20, and 1% DMSO \mp 100 μ M NADH with four variable concentrations of compound **13**. The contact time was 120 s, the dissociation time was 300 s, and the flow rate was 50 μ L/min. Data evaluation and fitting were performed with Biacore Insight Evaluation Software.

Docking and Binding Site Characterization. All calculations were performed using the Schrödinger Suite molecular modeling package (release 2019-2, Maestro, Schrödinger, LLC, New York, NY). The crystal structure of Mtb Lpd in complex with **1a** (PDB 4M52) was used for docking studies.⁸ The structure was prepared using the Protein Preparation Wizard with default settings. Waters with fewer than three hydrogen bonds to nonwaters were removed. A receptor grid centered at the centroid of co-crystallized compound **1a**, which can accommodate ligands with lengths of up to 20 \AA , was generated. New ligands were prepared using LigPrep and docked using Glide XP. The binding site region of **1a** plus a 6 \AA buffer area was evaluated by SiteMap.

■ ASSOCIATED CONTENT

Supporting Information

The Supporting Information is available free of charge at <https://pubs.acs.org/doi/10.1021/acsinfecdis.0c00788>.

Additional experimental data for Mtb Lpd recovery at different concentrations of **13**; Lpd co-crystal structure with **13** superimposed on the co-crystal with **1a**; ITC and SPR data; X-ray crystallography data collection and refinement statistics for the Mtb Lpd/compound **13** co-crystal; and details on chemical synthesis and compound purity (PDF)

■ AUTHOR INFORMATION

Corresponding Author

Ruslana Bryk – Department of Microbiology and Immunology, Weill Cornell Medicine, New York 10065, United States; orcid.org/0000-0002-2179-671X; Phone: 646-962-6207; Email: rub2001@med.cornell.edu

Authors

John Ginn – Tri-Institutional Therapeutics Discovery Institute, New York 10065, United States

Xiuju Jiang – Department of Microbiology and Immunology, Weill Cornell Medicine, New York 10065, United States

Shan Sun – Tri-Institutional Therapeutics Discovery Institute, New York 10065, United States

Mayako Michino – Tri-Institutional Therapeutics Discovery Institute, New York 10065, United States

David J. Huggins – Tri-Institutional Therapeutics Discovery Institute, New York 10065, United States; Department of Physiology and Biophysics, Weill Cornell Medicine, New York 10065, United States; orcid.org/0000-0003-1579-2496

- Zodwa Mbambo – Department of Medicine, Weill Cornell Medicine, New York 10065, United States
- Robert Jansen – Department of Medicine, Weill Cornell Medicine, New York 10065, United States
- Kyu Y. Rhee – Department of Medicine, Weill Cornell Medicine, New York 10065, United States
- Nancy Arango – Structural Biology Program, Sloan Kettering Institute, New York 10065, United States
- Christopher D. Lima – Structural Biology Program, Sloan Kettering Institute, New York 10065, United States; Howard Hughes Medical Institute, New York 10065, United States; orcid.org/0000-0002-9163-6092
- Nigel Liverton – Tri-Institutional Therapeutics Discovery Institute, New York 10065, United States
- Toshihiro Imaeda – Tri-Institutional Therapeutics Discovery Institute, New York 10065, United States
- Rei Okamoto – Tri-Institutional Therapeutics Discovery Institute, New York 10065, United States
- Takanobu Kuroita – Tri-Institutional Therapeutics Discovery Institute, New York 10065, United States
- Kazuyoshi Aso – Tri-Institutional Therapeutics Discovery Institute, New York 10065, United States
- Andrew Stamford – Tri-Institutional Therapeutics Discovery Institute, New York 10065, United States
- Michael Foley – Tri-Institutional Therapeutics Discovery Institute, New York 10065, United States
- Peter T. Meinke – Tri-Institutional Therapeutics Discovery Institute, New York 10065, United States
- Carl Nathan – Department of Microbiology and Immunology, Weill Cornell Medicine, New York 10065, United States

Complete contact information is available at:
<https://pubs.acs.org/10.1021/acsinfecdis.0c00788>

Funding

This work was supported by NIH grant R01 AI064768 to CN and the Abby and Howard P. Milstein Program in Chemical Biology and Translational Medicine at WCM. This work was also supported in part by NIH grant R35 GM118080 (CDL) and NIH National Cancer Institute-Cancer Center Support Grant P30 CA008748. The work presented here was also based in part on research conducted at the NE-CAT beamlines (NIH NIGMS Grant P41 GM103403 and NIH Office of Research Infrastructure Programs High-End Instrumentation Grant S10 RR029205). Beamline research used resources of the APS, a US Department of Energy (DOE) Office of Science User Facility operated for the DOE Office of Science by Argonne National Laboratory under Contract DE-AC02-06CH11357. The content is solely the responsibility of the authors and does not represent the official views of the NIH. CDL is an Investigator of the Howard Hughes Medical Institute. The Department of Microbiology & Immunology is supported by the William Randolph Hearst Trust. The authors gratefully acknowledge the generous support to this project (not to the non-TDI laboratories) provided by the Tri-Institutional Therapeutics Discovery Institute (TDI), a 501(c)(3) organization. TDI receives financial support from Takeda Pharmaceutical Company, TDI's parent institutes (Memorial Sloan Kettering Cancer Center, The Rockefeller University and Weill Cornell Medicine) and from a generous contribution from Mr. Lewis Sanders and other philanthropic sources.

Notes

The authors declare no competing financial interest.

ACKNOWLEDGMENTS

We thank our colleagues Leigh Baxt, Stacia Kargman, Robert Myers, and Gang Lin for their critical comments and discussions. For the expert technical help with ITC and SPR, we thank Carolina Adura Alcaino, Lavoisier Ramos-Espiritu, Fraser Glickman, and the Rockefeller University HTSRC. For the SPR data analysis, we thank Michael Murphy (Cytiva). We thank Yan Ling for help with protein purification and Daniel Pfau for the isolation of mouse primary bone marrow macrophages.

ABBREVIATIONS

ADME, absorption, distribution, metabolism, and excretion; ADN, albumin, dextrose, NaCl media supplement; AhpC, alkyl hydroperoxide reductase subunit C; AhpD, alkyl hydroperoxide reductase subunit D; BMDM, bone-marrow-derived macrophage; BPaL, bedaquiline, pretomanid, and linezolid regimen; CFU, colony-forming units; CoA, coenzyme A; DTNB, 5,5'-dithiobis-2-nitrobenzoic acid; HEPG2, human hepatocyte cell line; hLM, human liver microsomes; IFN γ , interferon γ ; IC₅₀, half-maximal inhibitory concentration; ITC, isothermal titration calorimetry; LC-MS, liquid chromatography-mass spectrometry; Lpd, lipoamide dehydrogenase; MIC, minimal inhibitory concentration; MDR, multi-drug-resistant; MOI, multiplicity of infection; Mtb, *Mycobacterium tuberculosis*; PDH, pyruvate dehydrogenase; PK, pharmacokinetics; RT, room temperature; SAR, structure-activity relationship; SPR, surface plasmon resonance; MTS, tetrazolium-based cell toxicity assay; TB, tuberculosis; TNB, 5-thio-2-nitrobenzoic acid; WT, wild type; XDR, extensively drug-resistant

REFERENCES

- (1) WHO. *Global Tuberculosis Reports*; WHO: https://www.who.int/tb/publications/global_report/en/, 2019.
- (2) Tian, J., Bryk, R., Shi, S., Erdjument-Bromage, H., Tempst, P., and Nathan, C. (2005) *Mycobacterium tuberculosis* appears to lack alpha-ketoglutarate dehydrogenase and encodes pyruvate dehydrogenase in widely separated genes. *Mol. Microbiol.* 57 (3), 859–68.
- (3) Venugopal, A., Bryk, R., Shi, S., Rhee, K., Rath, P., Schnappinger, D., Ehrhart, S., and Nathan, C. (2011) Virulence of *Mycobacterium tuberculosis* depends on lipoamide dehydrogenase, a member of three multienzyme complexes. *Cell Host Microbe* 9 (1), 21–31.
- (4) Bryk, R., Griffin, P., and Nathan, C. (2000) Peroxynitrite reductase activity of bacterial peroxiredoxins. *Nature* 407 (6801), 211–5.
- (5) Bryk, R., Lima, C. D., Erdjument-Bromage, H., Tempst, P., and Nathan, C. (2002) Metabolic enzymes of mycobacteria linked to antioxidant defense by a thioredoxin-like protein. *Science* 295 (5557), 1073–7.
- (6) Rajashankar, K. R., Bryk, R., Kniewel, R., Buglino, J. A., Nathan, C. F., and Lima, C. D. (2005) Crystal structure and functional analysis of lipoamide dehydrogenase from *Mycobacterium tuberculosis*. *J. Biol. Chem.* 280 (40), 33977–83.
- (7) Bryk, R., Arango, N., Venugopal, A., Warren, J. D., Park, Y. H., Patel, M. S., Lima, C. D., and Nathan, C. (2010) Triazaspirodime-thoxybenzoyls as selective inhibitors of mycobacterial lipoamide dehydrogenase. *Biochemistry* 49 (8), 1616–27.
- (8) Bryk, R., Arango, N., Maksymiuk, C., Balakrishnan, A., Wu, Y. T., Wong, C. H., Masquelin, T., Hipskind, P., Lima, C. D., and Nathan, C. (2013) Lipoamide channel-binding sulfonamides selectively inhibit mycobacterial lipoamide dehydrogenase. *Biochemistry* 52 (51), 9375–84.
- (9) Halgren, T. (2007) New method for fast and accurate binding-site identification and analysis. *Chem. Biol. Drug Des.* 69 (2), 146–8.

- (10) Friesner, R. A., Banks, J. L., Murphy, R. B., Halgren, T. A., Klicic, J. J., Mainz, D. T., Repasky, M. P., Knoll, E. H., Shelley, M., Perry, J. K., Shaw, D. E., Francis, P., and Shenkin, P. S. (2004) Glide: a new approach for rapid, accurate docking and scoring. 1. Method and assessment of docking accuracy. *J. Med. Chem.* 47 (7), 1739–49.
- (11) Tanner, L., Denti, P., Wiesner, L., and Warner, D. F. (2018) Drug permeation and metabolism in *Mycobacterium tuberculosis*: Prioritising local exposure as essential criterion in new TB drug development. *IUBMB Life* 70 (9), 926–937.
- (12) Smith, T. C., and Aldridge, B. B. (2019) Targeting drugs for tuberculosis. *Science* 364 (6447), 1234–1235.
- (13) Anderson, K., Lai, Z., McDonald, O. B., Stuart, J. D., Nartey, E. N., Hardwicke, M. A., Newlander, K., Dhanak, D., Adams, J., Patrick, D., Copeland, R. A., Tummino, P. J., and Yang, J. (2009) Biochemical characterization of GSK1070916, a potent and selective inhibitor of Aurora B and Aurora C kinases with an extremely long residence time. *Biochem. J.* 420 (2), 259–65.
- (14) Gopinathan, K. P., Sirsi, M., and Ramakrishnan, T. (1963) Nicotinamide-adenine nucleotides of *Mycobacterium tuberculosis* H37Rv. *Biochem. J.* 87, 444–8.
- (15) Boshoff, H. I., Xu, X., Tahlan, K., Dowd, C. S., Pethe, K., Camacho, L. R., Park, T. H., Yun, C. S., Schnappinger, D., Ehrhart, S., Williams, K. J., and Barry, C. E. (2008) Biosynthesis and recycling of nicotinamide cofactors in *Mycobacterium tuberculosis*. An essential role for NAD in nonreplicating bacilli. *J. Biol. Chem.* 283 (28), 19329–41.
- (16) Rao, S. P., Alonso, S., Rand, L., Dick, T., and Pethe, K. (2008) The protonmotive force is required for maintaining ATP homeostasis and viability of hypoxic, nonreplicating *Mycobacterium tuberculosis*. *Proc. Natl. Acad. Sci. U. S. A.* 105 (33), 11945–50.
- (17) Copeland, R. A., Pompliano, D. L., and Meek, T. D. (2006) Drug-target residence time and its implications for lead optimization. *Nat. Rev. Drug Discovery* 5 (9), 730–9.
- (18) Srinivasan, B., and Skolnick, J. (2015) Insights into the slow-onset tight-binding inhibition of *Escherichia coli* dihydrofolate reductase: detailed mechanistic characterization of pyrrolo [3,2-f] quinazoline-1,3-diamine and its derivatives as novel tight-binding inhibitors. *FEBS J.* 282 (10), 1922–38.
- (19) McClerren, A. L., Endsley, S., Bowman, J. L., Andersen, N. H., Guan, Z., Rudolph, J., and Raetz, C. R. (2005) A slow, tight-binding inhibitor of the zinc-dependent deacetylase LpxC of lipid A biosynthesis with antibiotic activity comparable to ciprofloxacin. *Biochemistry* 44 (50), 16574–83.
- (20) Cardona, F., Goti, A., Parmeggiani, C., Parenti, P., Forcella, M., Fusi, P., Cipolla, L., Roberts, S. M., Davies, G. J., and Gloster, T. M. (2010) Casuarine-6-O- α -D-glucoside and its analogues are tight binding inhibitors of insect and bacterial trehalases. *Chem. Commun. (Cambridge, U. K.)* 46 (15), 2629–31.
- (21) Svetlov, M. S., Vázquez-Laslop, N., and Mankin, A. S. (2017) Kinetics of drug-ribosome interactions defines the efficacy of macrolide antibiotics. *Proc. Natl. Acad. Sci. U. S. A.* 114 (52), 13673–13678.
- (22) Davoodi, S., Daryaei, F., Chang, A., Walker, S. G., and Tonge, P. J. (2020) Correlating Drug-Target Residence Time and Post-antibiotic Effect: Insight into Target Vulnerability. *ACS Infect. Dis.* 6 (4), 629–636.
- (23) Walkup, G. K., You, Z., Ross, P. L., Allen, E. K., Daryaei, F., Hale, M. R., O'Donnell, J., Ehmann, D. E., Schuck, V. J., Buurman, E. T., Choy, A. L., Hajec, L., Murphy-Benenato, K., Marone, V., Patey, S. A., Grosser, L. A., Johnstone, M., Walker, S. G., Tonge, P. J., and Fisher, S. L. (2015) Translating slow-binding inhibition kinetics into cellular and in vivo effects. *Nat. Chem. Biol.* 11 (6), 416–23.
- (24) Bryk, R., Gold, B., Venugopal, A., Singh, J., Samy, R., Pupek, K., Cao, H., Popescu, C., Gurney, M., Hotha, S., Cherian, J., Rhee, K., Ly, L., Converse, P. J., Ehrhart, S., Vandal, O., Jiang, X., Schneider, J., Lin, G., and Nathan, C. (2008) Selective killing of nonreplicating mycobacteria. *Cell Host Microbe* 3 (3), 137–45.
- (25) Adams, P. D., Afonine, P. V., Bunkoczi, G., Chen, V. B., Davis, I. W., Echols, N., Headd, J. J., Hung, L. W., Kapral, G. J., Grosse-
- Kunstleve, R. W., McCoy, A. J., Moriarty, N. W., Oeffner, R., Read, R. J., Richardson, D. C., Richardson, J. S., Terwilliger, T. C., and Zwart, P. H. (2010) PHENIX: a comprehensive Python-based system for macromolecular structure solution. *Acta Crystallogr., Sect. D: Biol. Crystallogr.* 66 (Pt 2), 213–221.
- (26) Emsley, P., and Cowtan, K. (2004) Coot: model-building tools for molecular graphics. *Acta Crystallogr., Sect. D: Biol. Crystallogr.* 60, 2126–2132.
- (27) Chen, V. B., Arendall, W. B., III, Headd, J. J., Keedy, D. A., Immormino, R. M., Kapral, G. J., Murray, L. W., Richardson, J. S., and Richardson, D. C. (2010) MolProbity: all-atom structure validation for macromolecular crystallography. *Acta Crystallogr., Sect. D: Biol. Crystallogr.* 66 (Pt 1), 12–21.